OPEN

VO_2 thermochromic smart window for energy savings and generation

Jiadong Zhou[1,2], Yanfeng Gao[1,2], Zongtao Zhang[3], Hongjie Luo[1,2], Chuanxiang Cao[2], Zhang Chen[2], Lei Dai[2] & Xinling Liu[2]

[1]School of Materials Science and Engineering, Shanghai University, Shangda Rd. 99, Baoshan, Shanghai 200444, China, [2]Shanghai Institute of Ceramics (SIC), Chinese Academy of Sciences (CAS), Dingxi 1295, Changning, Shanghai, 200050, China, [3]School of Materials Science and Engineering, Zhengzhou University, Zhengzhou 450001, China.

The ability to achieve energy saving in architectures and optimal solar energy utilisation affects the sustainable development of the human race. Traditional smart windows and solar cells cannot be combined into one device for energy saving and electricity generation. A VO_2 film can respond to the environmental temperature to intelligently regulate infrared transmittance while maintaining visible transparency, and can be applied as a thermochromic smart window. Herein, we report for the first time a novel VO_2-based smart window that partially utilises light scattering to solar cells around the glass panel for electricity generation. This smart window combines energy-saving and generation in one device, and offers potential to intelligently regulate and utilise solar radiation in an efficient manner.

Most efforts to efficiently utilise solar energy have been focused on improving the efficiency in the conversion and storage using solar cells[1–7] and large capacity batteries[8], respectively. However, these cells, which have been used on housetops and wall periphery, could not be integrated into windows that require the material to be transparent. Traditionally designed energy-saving windows, such as electrochromic thermochromic, and gasochromic, typically function by exterior stimuli involving either an electric field, heat stimulus or a gas[9]. It is not possible to alter the optical performance, which involves intelligently passing or blocking solar energy in response to environmental changes, and simultaneously generate electricity[10,11]. Herein, a novel smart window was designed such that the VO_2 films or particles regulate solar infrared radiation and scatter partial light to a solar cell for electricity generation.

It is known that VO_2 undergoes a fully reversible metal-semiconductor transition (MST) at a critical temperature (T_c) of $68°C$[12]. Below T_c ($T<T_c$), VO_2 is a monoclinic crystalline structure, which is insulating and transparent to infrared light, but it becomes a tetragonal crystalline structure that is metallic and reflective to infrared light above T_c ($T>T_c$)[13,14]. This phase transition property makes VO_2 an attractive material for smart windows[15]. Current research efforts have been primarily focused on enhancing the optical properties of VO_2 films (e.g., the improvement of the solar energy modulation ability and visible transmittance of VO_2 using multi-layered structures by designing high-reflective-index dielectric top or under layers (i.e., SiO_2/VO_2[16,21], TiO_2/VO_2[17] and $In_2O_3:Sn/VO_2/In_2O_3:Sn$[18]), forming nanoparticle composite foils (i.e., SiO_2/VO_2 core-shell[19], VO_2/ATO[20]) or enhancing the visible transmittance by doping (i.e., F-doped VO_2[21] and Mg-doped VO_2[22]). The focal points of the above-mentioned studies involve changing the transmittance, absorption and reflection characteristics of VO_2. However, the scattering interaction between the material and light has been ignored, resulting in a loss of the energy associated with scattering.

Results

Three devices that can save energy and simultaneously generate electricity were designed. Scattering can be defined as Tyndall, Mie or Rayleigh types based on the interactional relationship between wavelength (λ) of light and size of material, which implies the possibility to size-dependent control the strength of scattering[23]. A finite-difference-time-domain (FDTD) algorithm is useful for designing and investigating a varieties of devices and applications involving the propagation of electromagnetic radiation through complicated media, and was employed to investigate the interaction between VO_2 particles and light (Figure 1a). The electric field distribution of different particle sizes with light[24] (Figures 1b through 1f) indicates that light bypasses the particle propagation and that the scattering is so weak at a VO_2 particle size of less than 50 nm. However, the scattering is significantly enhanced with an increase in the particle size (i.e., 100 nm, 150 nm, 200 nm and
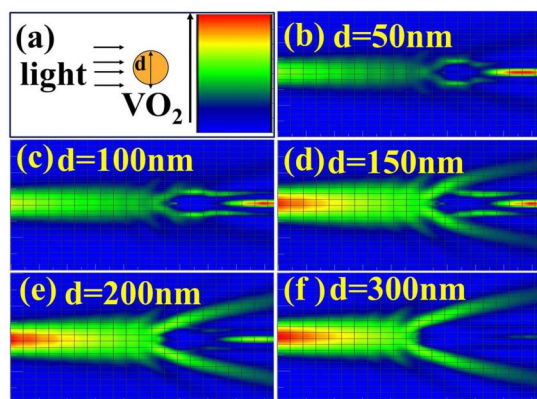
Figure 1 | The scatter electric field distribution of the interaction between a single VO$_2$ particle and light was simulated by FDTD. (a), The interaction of a single VO$_2$ particle with light, where the colour represents the incident light. The particle size of VO$_2$ is 50, 100, 150, 200 and 300 nm for (b, c, d, e and f), respectively. The scattering was enhanced as the particle size increased.

300 nm). The scattering behaviour between VO$_2$ particle arrays and light was further simulated by FDTD to illustrate the potential use of scattered light for electricity generation (Figure 2). In this simulation, both the radius of the VO$_2$ particle and the distance between two particles are 100 nm. The scattering of normal incident light in a wavelength range of 350–780 nm along the z-direction and polarised along the y/x-direction was simulated[25] (Figure 2a). The far field angular scattering shown in Figure 2b suggests that the scattering field intensity extended to a far zone, which means the scattering field is obvious and large. The scattering energy distribution in the y-z plane is larger than that in the x-y plane, which changed the transmittance of the film in x-y plane.

Based on this model, a solar cell module possessing energy-saving characteristics was designed and is shown in Figures 3a–3d. The structure consisted of three sections, including a low reflective index medium (e.g., VO$_2$-based particle or film), light guider layers and solar cells. To collect scattered light using this structure, the light guider layers should have a high reflective index associated with the reflective material, which enables the scattering light to propagate between the light guider layers and be reflected to the solar cells. The total internal reflection occurs when light propagates into an optically thinner medium from a denser medium with an incident angle larger than the total internal reflection angle c. The VO$_2$-based particle can scatter some of light to solar cells for generation.

In Figure 3e–3f, the three devices (i.e., C$_a$, C$_b$ and C$_c$) have been designed, a polycarbonate plate (PC plate, refractive index: 1.59) is employed as the light guider layer to gather scattering light to polysilicon solar cells. In Figure 3e-C$_a$, the low reflective index medium for the device C$_a$ (Figure 3b) and C$_b$ (Figure 3c) was a VO$_2$ particle film on a quartz plate and VO$_2$-based power arrays, respectively. The latter was designed as a core-shell-shell structure (i.e., VO$_2$@SiO$_2$@TiO$_2$) to decrease the absorption of VO$_2$ while maintaining the overall size of the particles to fulfil the scattering conditions[26]. In Figure 3f, the low reflective index medium for the device C$_c$ (Figure 3d) was a smooth VO$_2$ thin film. The thickness of the PC is about 4 mm and thickness of the low reflective index medium is about 200 nm in these devices.

Discussion

Figure 4 shows the optical scattering spectra, the transmittance spectra and the *I-V* curves of devices C$_a$, C$_b$ and C$_c$. The scattering measured by the bidirectional reflectance distribution function (BRDF) method[27] indicated that the scattering of C$_a$ is larger than C$_b$ and C$_c$ (Figure 4a) because the absorption of the film cast in PDMS for the C$_b$ is enhanced. The scattering of C$_c$ that used a smooth thin film as medium decreased, and the corresponding value of the BRDF for C$_c$ is lower than C$_a$ and C$_b$. The BRDF curve is consistent with the simulation of FDTD, which indicates that the scattering is large enough for generation. Figure 4b shows the optical transmittance spectra of C$_a$, C$_b$ and C$_c$ before and after the MST. Consistently, the transmittance in the wavelength range of 300–1,000 nm for the device C$_a$ at a high temperature (i.e., 90°C) is higher than that at a low temperature (i.e., 25°C), which is due to the enhanced scattering while the absorption is weakened. In addition, the transmittance of C$_a$ is higher than that of C$_b$ due to the structural difference.
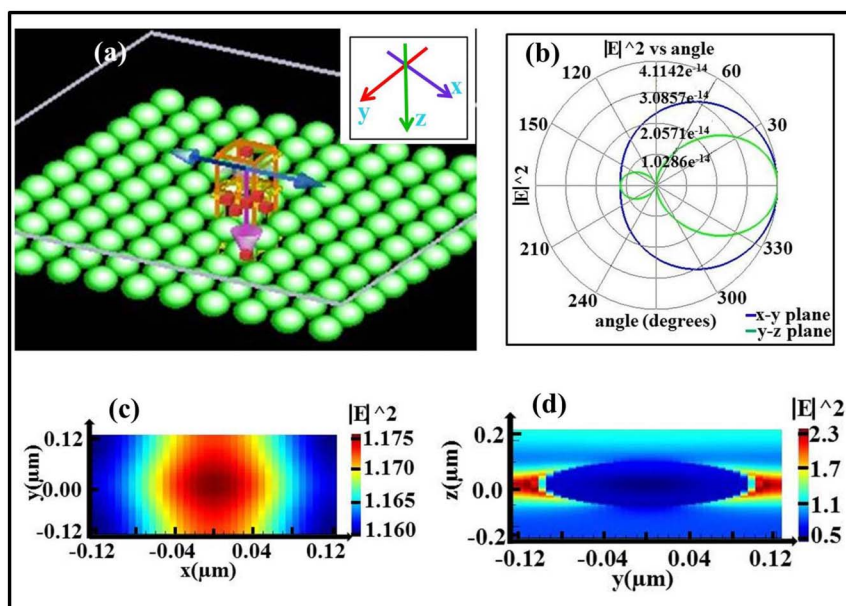

Figure 2 | The scattering of a VO$_2$ particle arrays film and the electric field intensity profiles of scattered light were simulated. (a), The simulation scheme (inset shows coordinate directions). The normal incident light was along the z-direction and polarised along the y/x-direction. (b), Far field angular scattering, which shows the behaviour of the scattered field in the far zone in the x-y and y-z planes. The vertical direction numbers represent the relative intensity. (c and d), The electric field intensity scattered by the VO$_2$-based particle film is indicated by a colour scale in the x-y and y-z planes.
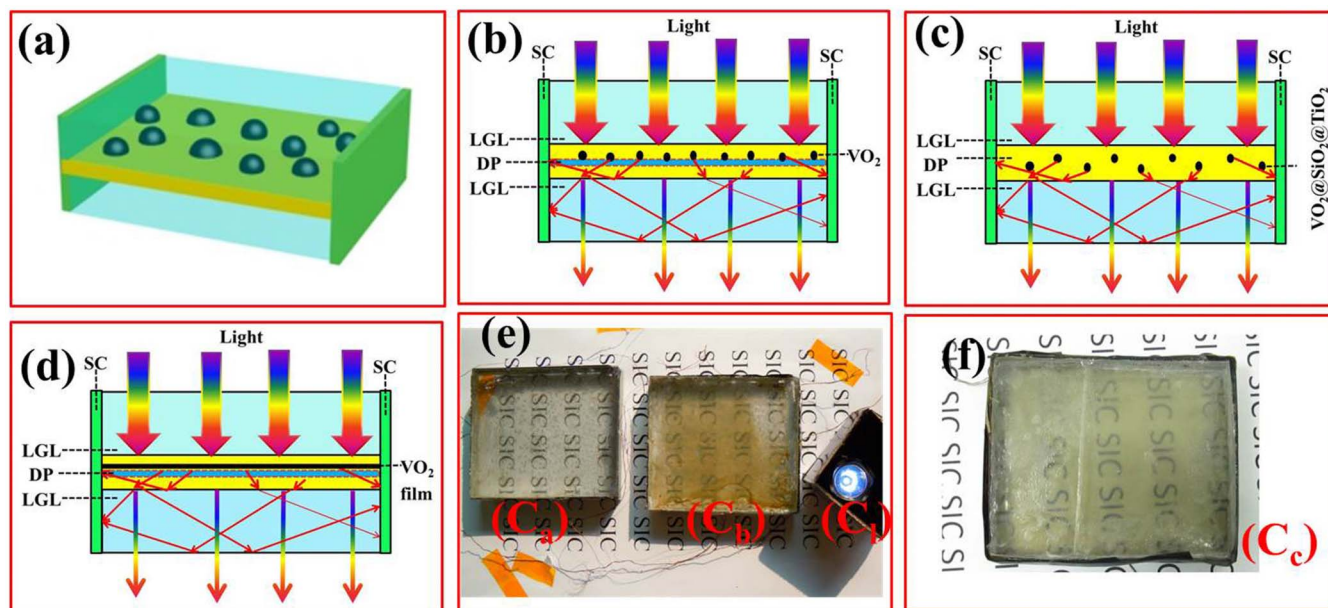
Figure 3 | The work principle scheme and the structure description of the VO$_2$-based thermochromic/generating smart window. (a), Three-dimensional structure of the prepared VO$_2$-based smart window. The solar cells are assembled in a manner that surrounds the module. Here, 3 sides are shown. (b), c and d are the cross-sectional views of a with different DP. (b), A VO$_2$ film on quartz that served as a scattering medium. The scattering medium in c is a composite created by the dispersion of VO$_2$@SiO$_2$@TiO$_2$ core-shell-shell particles in PU. This composite is cast in PDMS. The scattering medium in d is a smooth VO$_2$ thin film. SC, LGL and DP refer to the solar cell, light guider layer and low reflective index medium, respectively. (b, c and d) show the principle scheme of the devices C$_a$, C$_b$ (Figure 3e) and C$_c$ (Figure 3f), respectively. When light interacts with the VO$_2$ particle, partial light was scattered and reflected to the solar cell to generate electricity. C$_l$ is a 1.5-V lamp, which was employed to demonstrate whether the smart window works for generation. The two devices in series in Figure 3e could light a 1.5 V lamp.

To investigate the optical properties of the devices, the solar modulation efficiency (ΔT_{sol}) was calculated to characterise the thermochromic smart window properties of the devices. T_{vis} denotes the integral visible transmittance of the devices. The calculated results of the three devices are shown in Table 1. These results indicate that the ΔT_{sol} of the C$_a$ is only 2.0%, and the T_{vis} values at high and low temperatures are 65.6% and 61.7%, respectively. The ΔT_{sol} of C$_b$ is 7.5%, which is much higher than C$_a$, and the T_{vis} values at high and low temperatures are 45.6% and 42.7%, respectively. The results suggest that the VO$_2$-based core-shell-shell structure is beneficial for energy saving. For the C$_c$ with a smooth VO$_2$ thin film, the solar energy modulation ability of VO$_2$ was maintained.

The I-V curves are shown in Figure 4c, and the results are summarised in Table 2. The C$_a$ and C$_b$ devices show efficiencies of 0.50% and 0.52%, V_{oc} values of 0.501 V and 0.498 V, FF values of 50.18% and 59.68% and J_{sc} values of 2.0 mA/cm^2 and 1.74 mA/cm^2 for C$_a$ and C$_b$, respectively. The efficiency and FF values of C$_b$ are higher than those of C$_a$, which shows that the C$_b$ structure is more efficient compared to that of C$_a$ in terms of gathering scattering energy. Note that the area of C$_a$ is large than C$_b$, so the scattering light in C$_a$ attenuated bigger than that in C$_b$. The properties of the device C$_c$ are worse than C$_a$ and C$_b$, probably because of decreased scattering.

Buildings and other man-made structures consume 30–40% of the primary energy for heating, cooling, ventilation and lighting. This phenomenon will increase with the growth of the population and the associated energy consumption[28]. The ability to reduce energy consumption has become an urgent priority. The successful design and preparation of a novel smart window that combines energy-saving and electricity generation achieves comprehensive utilisation of solar energy, which supports an important new insight into resolving the energy consumption.
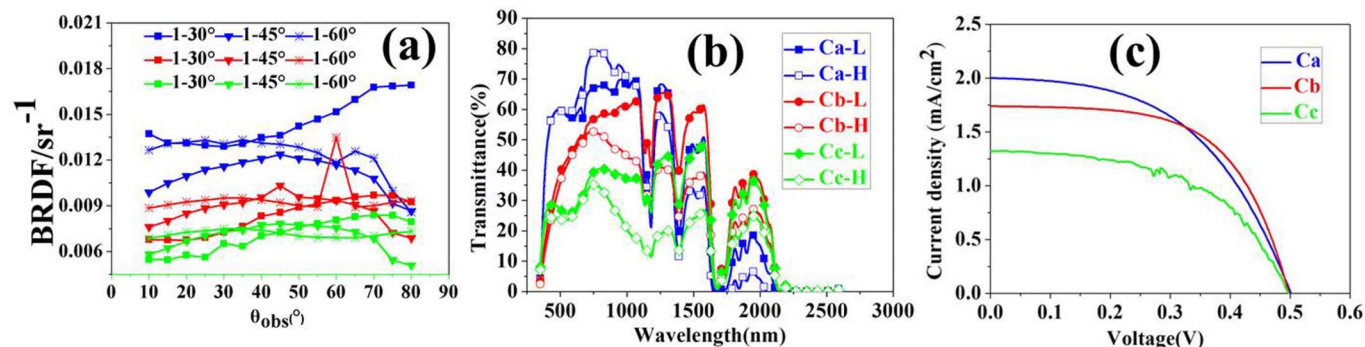

Figure 4 | The results of the BRDF curve, transmittance spectra of three windows and I-V curves of the three devices. In Figure 4a, the BRDF curve under the measurement conditions has a polarisation incidence with an incident wavelength of 635 nm. C$_a$, C$_b$ and C$_c$ represent the curve of the C$_a$, C$_b$ and C$_c$ devices in Figure 3e and 3f, respectively. The incident angle was fixed at 30°, 45° and 60°, and the intensity of the reflective light was measured from 10° to 80°. The results indicate that the scattering intensity of C$_a$ is larger than C$_b$ and C$_c$. In the Figures 4b and 4c, the optical transmittance spectra at low and high temperatures and the I-V curves under AM 1,5 illumination of the three devices in Figure 3e (C$_a$, and C$_b$) and 3f-C$_c$ are shown.

Table 1 | The visible transmittance, solar energy transmittance and solar modulation ability of the windows in Figure 3e and 3f

Sample	Visible transmittance T_{vis} (%)		Solar Transmittance T_{sol} (%)		Solar modulation ability (%)
	25°C	90°C	25°C	90°C	
C_a	61.7	65.6	56.2	58.2	2.0
C_b	45.6	42.7	46.9	39.3	7.5
C_c	31.5	28.0	32.1	24.1	8.0

Methods

Preparation of VO₂ films using a solution-based process. The thermochromic VO_2 films were prepared according to a previously reported protocol[29]. Vanadium pentoxide (V_2O_5, analytically pure), diamide hydrochloride ($N_2H_4 \cdot HCl$, analytically pure) and PVP (K90, average molecular weight: 1,300,000) were used as starting materials to prepare vanadium precursors. Quartz glass was used as the substrate and was subsequently cleaned in H_2O_2, HCl, and $NH_3 \cdot H_2O$. Precursor films were prepared by shin-coating at 3,000 rpm for 40 s. Then, the films were annealed at 520 in an N_2 (100%) and N_2-O_2 flow (N_2: 99.5%, O_2 0.5%) to prepare the smooth VO_2 thin film and VO_2 particle film, respectively.

Preparation of the VO₂@SiO₂@TiO₂/PU composite film. *Preparation of VO₂ nanoparticles.* The VO_2 nanoparticles were synthesised using the hydrothermal method according to a previously reported protocol[30]. In a typical procedure, vanadium pentoxide (V_2O_5, analytically pure) powder was added to an oxalic acid dehydrate aqueous solution to form a yellowish slurry. Then, the slurry was transferred to a 50 mL teflon-lined stainless-steel autoclave, which was maintained at 240°C for 24 h, and was then air-cooled to room temperature.

Preparation of VO₂@SiO₂ nanoparticles. First, VO_2 nanoparticles were pretreated with poly(vinylpyrrolidone) (PVP) K-30. Then, the VO_2@SiO₂ core-shell structure was prepared by the hydrolysis of TEOS, which is known as the modified Stöber growth method. Finally, the prepared sample was collected by centrifugation and washed with deionised water and ethanol several times[19].

Preparation of VO₂@SiO₂@TiO₂ nanoparticles. First, the as-prepared VO_2@SiO₂ nanoparticles were dispersed in an ethanol solution under strong stirring for 30 min. Then, the required amount of tetrabutyl titanate (TBOT) was quickly added. Finally, an ethanol solution containing 0.03 mL of $NH_3 \cdot H_2O$ was added drop-wise to the solution over 5 min. The reaction was maintained at 45°C for 24 h. When the reaction was complete, the sample was collected by centrifugation, washed with deionised water and ethanol several times, and dried at 50°C for 6 h[31].

Please see the reference for further information on the preparation of VO_2 nanoparticles and VO_2@SiO₂ nanoparticles[19].

Preparation of VO₂@SiO₂@TiO₂/PU composite film. The as-prepared particles were ultrasonically dispersed in deionised water and an appropriate amount of the saline coupler KH-570 was added under stirring. To this solution, the organic matrix material, polyurethane (PU, DISPERCOLLU 54, Bayer), was added with stirring for 10 min. Finally, the mixture was uniformly cast onto a PC substrate using an automatic coating machine and then dried to prepare the VO_2 solar cell.

Preparation of VO₂-based solar cells. The VO_2 smart window solar cells were assembled according to the structure in Figure 3. The PC plate was used as the light guider layer. The low reflective index medium, VO_2-based film or nanoparticles with PDMS were adhered on the PC plate, and another PC plate was adhered on the low reflective index medium. After that, the silicon solar cells were adhered with PDMS. All of the cells were connected in parallel and the device was installed.

Characterization. The morphology of the VO_2 film was determined by field emission scanning electron microscopy (FESEM, JEOL Corp., Model JSM-6700F). The VO_2 nanoparticles were observed using transmission electron microscopy (TEM) and energy dispersive spectrometry (EDS, JEM2010F, JEOL, Japan), and the VO_2 film was observed using transmission electron microscopy (TEM). The phase identification was obtained via X-ray diffraction (XRD, Model D/Max 2550 V, Rigaku, Japan, Cu Kα, $\lambda = 0.15406$ nm). The transmittance spectra at normal incidence from 240 nm to 2600 nm were measured using a Hitachi U-4100 spectrometer. The scattering interaction between the VO_2 particles and light was simulated by the finite difference time domain solution (FDTD). The scattering of the VO_2-based smart windows was measured using the method of the bidirectional reflectance distribution function.

1. Chu, S. & Majumdar, A. Opportunities and challenges for a sustainable energy future. *Nature* **488**, 294–303 (2012).
2. Tomabechi, K. Energy Resources in the Future. *Energies* **3**, 686–695 (2010).
3. Peng, K. Q. & Lee, S. T. Silicon Nanowires for Photovoltaic Solar Energy Conversion. *Adv. Mater.* **23**, 198–215 (2011).
4. Chopra, K. L., Paulson, P. D. & Dutta, V. Thin-film solar cells: An overview. *Prog. Photovoltaics* **12**, 69–92 (2004).
5. Shah, A., Torres, P., Tscharner, R., Wyrsch, N. & Keppner, H. Photovoltaic technology: The case for thin-film solar cells. *Science* **285**, 692–698 (1999).
6. Chung, I., Lee, B., He, J. Q., Chang, R. P. H. & Kanatzidis, M. G. All-solid-state dye-sensitized solar cells with high efficiency. *Nature* **485**, 486–494 (2012).
7. Graetzel, M., Janssen, R. A. J., Mitzi, D. B. & Sargent, E. H. Materials interface engineering for solution-processed photovoltaics. *Nature* **488**, 304–312 (2012).
8. Blom, P. W. M., Mihailetchi, V. D., Koster, L. J. A. & Markov, D. E. Device physics of polymer: fullerene bulk heterojunction solar cells. *Adv. Mater.* **19**, 1551–1566 (2007).
9. Baetens, R., Jelle, B. P. & Gustavsen, A. Properties, requirements and possibilities of smart windows for dynamic daylight and solar energy control in buildings: A state-of-the-art review. *Sol. Energy. Mater. Sol. Cells* **94**, 87–105 (2010).
10. Cheng, F. Y., Liang, J., Tao, Z. L. & Chen, J. Functional Materials for Rechargeable Batteries. *Adv. Mater.* **23**, 1695–1715 (2011).
11. Li, S. Y., Niklasson, G. A. & Granqvist, C. G. Thermochromic fenestration with VO_2-based materials: Three challenges and how they can be met. *Thin. Solid. Films* **520**, 3823–3828 (2012).
12. Qazilbash, M. M. *et al.* Mott transition in VO_2 revealed by infrared spectroscopy and nano-imaging. *Science* **318**, 1750–1753 (2007).
13. Liu, M. K. *et al.* Terahertz-field-induced insulator-to-metal transition in vanadium dioxide metamaterial. *Nature* **487**, 345–348 (2012).
14. Nakano, M. *et al.* Collective bulk carrier delocalization driven by electrostatic surface charge accumulation. *Nature* **487**, 459–462 (2012).
15. Lee, M. H. Thermochromic glazing of windows with better luminous solar transmittance. *Sol. Energy. Mater. Sol. Cells* **71**, 537–540 (2002).
16. Chen, Z. *et al.* VO_2-based double-layered films for smart windows: Optical design, all-solution preparation and improved properties. *Sol. Energy. Mater. Sol. Cells* **95**, 2677–2684 (2011).
17. Jin, P., Xu, G., Tazawa, M. & Yoshimura, K. A VO_2-based multifunctional window with highly improved luminous transmittance. *Jpn. J. Appl. Phys.* **41**, L278–L280 (2002).
18. Heinilehto, S. T., Lappalainen, J. H., Jantunen, H. M. & Lantto, V. IR-wavelength optical shutter based on ITO/VO_2/ITO thin film stack. *J. Electroceram.* **27**, 7–12 (2011).
19. Gao, Y. F. *et al.* Enhanced chemical stability of VO_2 nanoparticles by the formation of SiO₂/VO_2 core/shell structures and the application to transparent and flexible VO_2-based composite foils with excellent thermochromic properties for solar heat control. *Energ. Environ. Sci.* **5**, 9947–9947 (2012).
20. Gao, Y. F. *et al.* VO_2-Sb:SnO₂ composite thermochromic smart glass foil. *Energ. Environ. Sci.* **5**, 8234–8237 (2012).
21. Burkhardt, W. *et al.* W- and F-doped VO_2 films studied by photoelectron spectrometry. *Thin. Solid. Films* **345**, 229–235 (1999).
22. Hu, S. L. *et al.* Optical properties of Mg-doped VO_2: Absorption measurements and hybrid functional calculations. *Appl. Phys. Lett.* **101**, 201902 (2012).
23. Hodkinso, Jr. Particle Sizing by Means of Forward Scattering Lobe. *Appl. Optics.* **5**, 839–844 (1966).
24. Goodenou, J.b. 2 Components of crystallographic transition in VO_2. *J. Solid State. Chem.* **3**, 490–4 (1971).
25. Zhao, J. *et al.* Methods for Describing the Electromagnetic Properties of Silverand Gold Nanoparticles. *Acc. Chem. Res.* **41**, 1710–1720 (2008).
26. Li, S. Y., Niklasson, G. A. & Granqvist, C. G. Nanothermochromics: Calculations for VO_2 nanoparticles in dielectric hosts show much improved luminous transmittance and solar energy transmittance modulation. *J. Appl. Phys.* **108**, (2010).
27. Schaaf, C. B. *et al.* First operational BRDF, albedo nadir reflectance products from MODIS. *Remote. Sens. Environ.* **83**, 135–148 (2002).

Table 2 | The efficiency, open-circuit voltage V_oc, fill factor FF and short-circuit current density J_sc under AM 1.5 illumination for three devices

cell	V_{oc} (V)	J_{sc} (mA/cm²)	FF (%)	Eff (%)	Area (cm²)
C_a	0.501	2.00	50.18	0.50	76
C_b	0.498	1.74	59.68	0.52	60
C_c	0.497	1.32	52.06	0.34	70

28. Rotzetter, A. C. C. *et al.* Thermoresponsive Polymer Induced Sweating Surfaces as an Efficient Way to Passively Cool Buildings. *Adv. Mater.* **24**, 5352–5356 (2012).
29. Zhang, Z. *et al.* Thermochromic VO_2 Thin Films: Solution-Based Processing, Improved Optical Properties, and Lowered Phase Transformation Temperature. *Langmuir* **26**, 10738–10744 (2010).
30. Cao, C. X., Gao, Y. F. & Luo, H. J. Pure Single-Crystal Rutile Vanadium Dioxide Powders: Synthesis, Mechanism and Phase-Transformation Property. *J. Phys. Chem. C* **112**, 18810–18814 (2008).
31. Li, W. *et al.* A Versatile Kinetics-Controlled Coating Method To Construct Uniform Porous TiO_2 Shells for Multifunctional Core-Shell Structures. *J. Am. Chem. Soc.* **134**, 11864–11867 (2012).

Acknowledgements

Author contributions

J.Z., Z.Z. and Y.G. designed the experiment. J.Z. performed synthesis experiments and characterization. Z.Z. and J.Z. performed simulation and analysis. J.Z. and Y.G. wrote the paper. J.Z., Z.Z., Y.G., H.L., C.C., Z.C., L.D. and X.L. contributed to analysis the experimental data.

Additional information

Supplementary information accompanies this paper at http://www.nature.com/scientificreports

Competing financial interests: The authors declare no competing financial interests.

How to cite this article: Zhou, J. *et al.* VO_2 thermochromic smart window for energy savings and generation. *Sci. Rep.* **3**, 3029; DOI:10.1038/srep03029 (2013).